



# Jahn-Teller distortion in bis(terpyridine)nickel(III) – Elongation or compression?

Jeanet Conradie <sup>a,b</sup>

<sup>a</sup> Department of Chemistry, University of the Free State, P.O. Box 339, Bloemfontein 9300, South Africa

<sup>b</sup> UiT - The Arctic University of Norway, N-9037 Tromsø, Norway

## ARTICLE INFO

**Keywords:**  
Nickel(III)  
Jahn-Teller  
DFT  
Terpyridine  
Orthorhombic distortion

## ABSTRACT

DFT methods were used to evaluate the type of Jahn-Teller distortion in the low spin  $d^7$  bis(terpyridine)nickel(III) doublet. The strain of the tridentate terpyridine ligand in bis(terpyridine)nickel(III) leads to longer Ni(III)-N terminal bond lengths than the Ni(III)-N central bonds. In addition, in all DFT optimized bis(terpyridine)nickel(III) molecules, the one set of Ni(III)-N terminal bonds are longer than the other set of Ni(III)-N terminal bonds. Three pairs of Ni(III)-N bonds are present in bis(terpyridine)nickel(III), namely 2 longer Ni(III)-N<sub>terminal1</sub> terminal bonds, 2 medium length Ni(III)-N<sub>terminal2</sub> terminal bonds and 2 shorter Ni(III)-N<sub>central</sub> central bonds, similar to orthorhombic Jahn-Teller distortion in octahedral complexes. Evaluation of bond length differences, contraction of bonds, spin density plots and the character of the singly occupied molecular orbital (SOMO) and singly unoccupied molecular orbital (SUMO), led to a set of criteria to consider in evaluating the type of Jahn-Teller distortion in the low spin  $d^7$  bis(terpyridine)nickel(III) doublet. Jahn-Teller distortion can lead to elongation (z-out) or compression (z-in) of a pair of opposite Ni-N bonds. One key criteria found, is, if the difference in bond length between Ni(III)-N<sub>terminal1</sub> and Ni(III)-N<sub>terminal2</sub> is smaller than the difference in bond length of Ni(III)-N<sub>terminal2</sub> and Ni(III)-N<sub>central</sub>, then it is a Jahn-Teller compression geometry (and vice versa for a Jahn-Teller elongation geometry).

## Introduction

Bis(terpyridine)nickel(II) complexes,  $[\text{Ni}(\text{tpy})_2]^{2+}$ , find various applications due to their unique properties. For example, Ni-terpyridine complexes catalyse C–C cross-coupling reactions [1], bis(terpyridine)nickel(II) acts as catalysts for the electrocatalytic reduction of  $\text{CO}_2$  [2,3] and bis(4'-(2-ferrocenyl)-2,2':6'2''-terpyridine)nickel(II) exhibit anti-amoebic and antimalarial activities [4]. Bis(terpyridine)nickel(II) complexes can serve as versatile building blocks in supramolecular chemistry [5,6], while bis(4'-(furan-2-yl)-2,2':6'2''-terpyridine)nickel(II) acts as precursor for the synthesis of nanoparticles [7]. Many  $[\text{Ni}(\text{tpy})_2]^{2+}$  molecules, as well as  $[\text{Ni}(\text{tpy})_2]^{2+}$  containing substituted terpyridine ligands, have been characterized by solid state crystallography [8–10], exhibiting a distorted or pseudo octahedral geometry due to the strain of the tridentate ligands [11,12]. However, no structure of the oxidized bis(terpyridine)nickel(III),  $[\text{Ni}(\text{tpy})_2]^{3+}$ , could be found [8–10].

Bis(terpyridine)nickel(III),  $[\text{Ni}(\text{tpy})_2]^{3+}$ , exhibits a Jahn-Teller distorted geometry due to the inequivalent electron occupation of degenerate d orbitals of the nickel ion [13,14]. The Jahn-Teller effect is a

phenomenon in which a molecule or complex distorts its geometry to lower its overall energy by removing degeneracy in the electronic energy levels [15]. In bis(terpyridine)nickel(III) complexes, the nickel ion is in the +3 oxidation state, resulting in the removal of one electron compared to the bis(terpyridine)nickel(II) complexes [3,16]. The electronic configuration of the nickel ion in bis(terpyridine)nickel(III) complexes is  $d^7$  [17]. The d orbitals of an isolated nickel ion are degenerate, meaning they have the same energy. However, in metal–ligand complexes, the interaction between the metal d-orbitals and the ligands leads to the splitting of the d-orbitals into different energy levels. In an octahedral ligand field, the splitting of the metal ion's d-orbitals results into two sets of orbitals, referred to as the  $t_{2g}$  (the  $d_{xy}$ ,  $d_{xz}$ , and  $d_{yz}$  orbitals) and  $e_g$  (the  $d_{x^2-y^2}$  and  $d_{z^2}$  orbitals) orbitals. The distorted octahedral  $d^7$  bis(terpyridine)nickel(III) complex with spin =  $1/2$ , has one electron in the  $e_g$  set of the d orbitals. The presence of an odd number of electrons in the  $e_g$  set leads to an electronic instability, and the complex undergoes a Jahn-Teller distortion to lower its energy [15]. The Jahn-Teller effect in octahedral  $d^7$  complexes typically results in elongation or compression of the coordination bonds, leading to a distortion of the octahedral geometry. This distortion breaks the degeneracy of the

E-mail address: [conradj@ufs.ac.za](mailto:conradj@ufs.ac.za).

<https://doi.org/10.1016/j.rechem.2023.101191>

Received 28 October 2023; Accepted 31 October 2023

Available online 6 November 2023

2211-7156/© 2023 The Author(s). Published by Elsevier B.V. This is an open access article under the CC BY-NC-ND license (<http://creativecommons.org/licenses/by-nc-nd/4.0/>).

d orbitals and reduces the electronic instability, stabilizing the complex. The Jahn-Teller distortion in octahedral complexes are most pronounced, can occur in different directions, resulting in different geometries. The distortion can cause the complex to become elongated along one axis, leading to a tetragonal elongation (z-out) geometry. Alternatively, it can cause a compression along one axis, resulting in a tetragonal compression (z-in) geometry [13]. Orthorhombic Jahn Teller distortion of an octahedron, with two opposite long, two opposite medium and two opposite short bonds, is also possible [18]. The Jahn-Teller distorted geometry in nickel(III) complexes could have implications for their properties and reactivity. It affects their spectroscopic features [19], magnetic properties [20], redox [21] and electron transfer [22] processes.

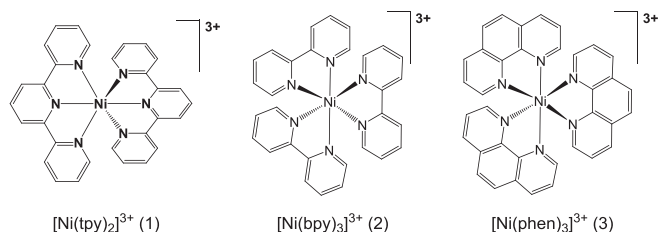
Understanding and characterizing the Jahn-Teller effect on the geometry of bis(terpyridine)nickel(III) complexes are important for the design and application of these complexes in various fields, including catalysis, magnetism, and molecular electronics. In this contribution, a DFT study on the Jahn-Teller distorted geometry of bis(terpyridine)nickel(III) is presented. For a full understanding of the DFT calculated structure of bis(terpyridine)nickel(III) (1), the DFT calculated structures of the related polypyridine complexes tris(bipyridine)nickel(III) (2) and tris(phenanthroline)nickel(III) (3) complexes are also discussed, see Scheme 1.

## Theoretical methods

Chemcraft [23] was utilized to construct the input coordinates for Density Functional Theory (DFT) calculations of compounds (1) - (3). DFT calculations were done on the molecules using the OLYP GGA (Generalized Gradient Approximation) functional [24,25] with or without Grimme's D3 dispersion correction [26]. The OLYP functional proved to correctly calculate the  $d_{z^2}^1$  versus the  $d_{x^2-y^2}^1$  ground state of Ni(III) for nickel(III) tetra(<sup>t</sup>butyl)porphyrin dicyanide [27]. Different basis sets were used:

- (i) The scalar relativistic ZORA (Zeroth Order Regular Approximation to the Dirac equation) Hamiltonian [28–30], and the ZORA TZ2P all-electron relativistic basis as implemented in the ADF program system [31,32] were used. This method will be referred to as the OLYP-D3/ZORA-TZ2P method (if Grimme's D3 dispersion correction was used) or OLYP/ZORA-TZ2P method (if no Grimme's D3 dispersion correction was used).
- (ii) The triple- $\zeta$  basis set 6-311G(d,p), as implemented in the Gaussian 16 package [33], was also used. This method will be referred to as the OLYP-D3/6-311G(d,p) or OLYP/6-311G(d,p), if D3 was used or not, respectively.

All molecules have undergone frequency analyses to guarantee the attainment of geometries with the lowest possible energy levels without any imaginary frequencies. All optimizations were in the gas phase.



**Scheme 1.** Structure, numbering and abbreviation of the polypyridine-nickel(III) molecules of this study. The highest symmetry point group possible for Jahn Teller distorted (1) is  $D_{2d}$  (for compression Jahn Teller distortion) or  $C_{2v}$  (for both elongation and compression Jahn Teller distortion). The highest symmetry point group possible for Jahn Teller distorted for (2) and (3) is  $C_2$ .

## Results and discussion

The 6-coordinated polypyridine-nickel(II) complexes of (1) – (3) have 8 d-electrons each with spin  $S = 1$  (triplet) [34–36]. Upon oxidation of the polypyridine-nickel(II) complexes of (1) – (3), polypyridine-nickel(III) complexes (1) – (3) are formed with 7 d-electrons each with either spin  $S = 1/2$  (doublet) or spin  $S = 3/2$ . Experimental and theoretical calculations showed that the ground state is  $S = 1/2$  [17,35,36]. The presence of a single unpaired electron in the  $e_g$  orbital set causes Jahn-Teller distortion in 6-coordinated pseudo octahedral nickel(III) complexes with 7 d-electrons [13,37]. Jahn-Teller distortion in octahedral complexes can cause the complex to become elongated along one axis (z-axis as defined in Fig. 1), leading to a Jahn-Teller elongated (z-out) geometry, or it can cause a compression along the z-axis, resulting in a Jahn-Teller compressed (z-in) geometry. On the Cambridge Structural Database (CSD [8–10]) only two Ni(III) crystals with a  $NiN_6$  coordination polyhedron exhibiting Jahn-Teller distortion, could be found. The solid state structure of tris(bipyridine)nickel(II) exhibits a compressed (z-in) Jahn-Teller geometry [35] with the axial Ni(III)-N bonds 0.1 Å shorter than the equatorial bonds. The solid state structure of bis(bis(1,4,7-triazacyclononane)-nickel(III)) [38] exhibits an elongated (z-out) Jahn-Teller geometry with the axial Ni(III)-N bonds 0.139 Å longer than the equatorial bonds. No structure of the bis(terpyridine)nickel(III) could be found.

### OLYP-D3/ZORA-TZ2P optimized geometries of (1) – (3)

In this section the optimized geometries and observed Jahn-Teller distortion, the spin density profile and important molecular orbitals (MOs), of (1) – (3), using the OLYP-D3/ZORA-TZ2P method, are discussed.

#### Geometry

The OLYP-D3/ZORA-TZ2P DFT calculated Ni-N bond lengths of the DFT calculated lowest energy ground state optimized geometries of (1) – (3), and their polypyridine-nickel(II) complexes, are summarized in Table 1.

Both tris(bipyridine)nickel(II) and tris(phenanthroline)nickel(II), each containing three bidentate ligands, have a pseudo octahedral geometry of symmetry  $D_3$ . The bidentate ligands reduce the molecular symmetry from octahedral  $O_h$  to  $D_3$  [39]. Under  $D_3$  symmetry, the six Ni(II)-N bonds of are all of the same length, 2.074 Å for tris(bipyridine)nickel(II) and 2.100 Å for tris(phenanthroline)nickel(II). However, in bis(terpyridine)nickel(II), strain of the tridentate terpyridine ligand causes the two central bonds to be shorter (1.996 Å) than the four terminal bonds (2.103 Å).  $D_3$  symmetry is not possible for bis(terpyridine)nickel(II), that optimized to a  $D_{2d}$  geometry. The two tridentate terpyridine ligands, arrange its six nitrogen atoms in a pseudo octahedral fashion around nickel(II). However, because of the spatial constraints imposed by the tridentate terpyridine ligand, the bis(terpyridine)nickel(II) pseudo octahedral system doesn't exhibit  $D_{4h}$  symmetry (dite-tragonal dipyramidal), but rather displays  $D_{2d}$  symmetry (tetragonal scalenohedral).

Upon oxidation of polypyridine-nickel(II), the Ni-N bond lengths change, some increase in length and some decrease in length. The presence of the single unpaired electron in the  $e_g$  orbital set after oxidation, causes Jahn-Teller distortion in the polypyridine-nickel(III) complexes, leading to a Jahn-Teller elongation or compression geometry (Fig. 1).

Evaluating the Ni(III)-N bond lengths of DFT optimized (2) and (3) in Table 1, it is clear that (2) and (3) exhibit Jahn-Teller elongation distortion with two long bonds along the z-axis direction and four short bonds in the xy-plane (xyz-axes are defined in Table 1). The two Ni(III)-N bonds of (2) and (3) in the z-direction are ca 0.18 Å longer than the four shorter Ni(III)-N bonds in the xy-plane, Fig. 2. On ground of the Ni(III)-N bond lengths, the Jahn-Teller distortion in the DFT optimized low

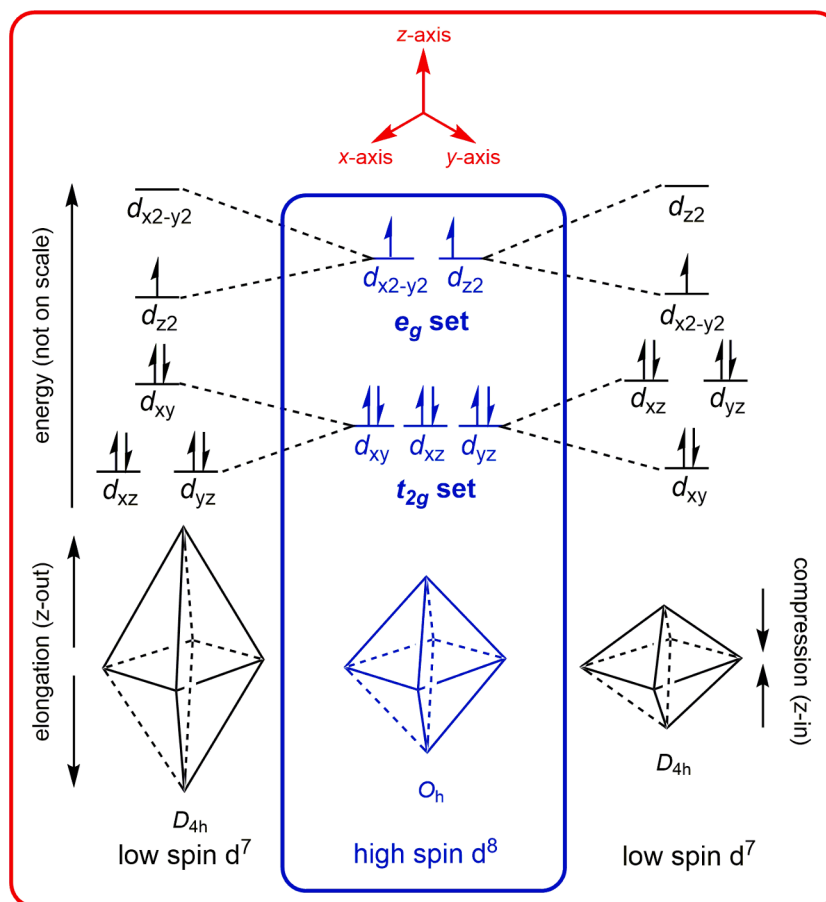


**Fig. 1.** Comparison between the d-orbital energies of low spin  $d^7$  complexes and high spin  $d^8$  octahedral complexes to demonstrate the impact of Jahn-Teller distortion on the geometry of low spin  $d^7$  complexes, leading to elongation (z-out) or compression (z-in) distortion.

spin  $d^7$  complexes (2) and (3), are Jahn-Teller elongation distortion.

Experimental structures of bis(terpyridine)nickel(II), containing two tridentate terpyridine ligands, are of  $D_{2d}$  symmetry (tetragonal crystal system, see CSD [8–10] reference codes FAGGOL [40], NUGHOP [41], YEZDIR [42]) or near to  $D_{2d}$  symmetry. The average Ni(II)-N terminal and central bonds of 28 structures bis(terpyridine)nickel(II) available on the CSD, are 2.111 and 1.993 Å respectively. The OLYP-D3/ZORA-TZ2P DFT calculated Ni(II)-N terminal and central bonds of bis(terpyridine)nickel(II) under  $D_{2d}$  symmetry, 2.103 and 1.996 Å respectively, are in perfect agreement with these average experimental values, validating the OLYP-D3/ZORA-TZ2P DFT are reliable to determine the properties of bis(terpyridine)nickel complexes. No structure of the oxidized bis(terpyridine)nickel(III),  $[\text{Ni}(\text{tpy})_2]^{3+}$ , could be found on the CSD [8–10].

The strain of the tridentate terpyridine ligand in bis(terpyridine)nickel(III), (1), causes the two central bonds in (1) to be shorter than the four terminal bonds, making the interpretation of the observed Jahn-Teller distortion difficult to evaluate on ground of the Ni(III)-N bond lengths. The highest symmetry point group possible for Jahn Teller distorted (1) is  $D_{2d}$  (tetragonal crystal system, for compression Jahn Teller distortion along the central bonds) or  $C_{2v}$  (orthorhombic crystal system, for both elongation and compression Jahn Teller distortion along opposite terminal bonds). All optimized geometries under  $D_{2d}$  symmetry, exhibited an imaginary frequency. For (1) optimized under  $C_{2v}$  symmetry, the OLYP-D3/ZORA-TZ2P optimized structure of (1) (see 1a in Table 1) has terminal bonds of 2.105 and 1.977 Å, and central constrained bonds of 1.882 and 1.848 Å (average of 1.865 Å). Thus, three pairs of Ni(III)-N bonds are present in bis(terpyridine)nickel(III), namely 2 longer Ni(III)-N<sub>terminal1</sub> terminal bonds, 2 medium length Ni(III)-N<sub>terminal2</sub> terminal bonds and 2 shorter Ni(III)-N<sub>central</sub> central bonds,

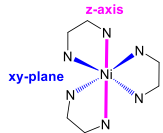
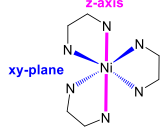
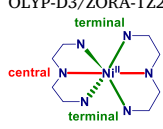
similar to orthorhombic Jahn-Teller distortion in octahedral complexes [18,43]. Orthorhombic Jahn-Teller distortion may lead to elongation (z-out) [21] or to compression (z-in) [44] of a pair of opposite bonds in an orthorhombic distorted octahedral complex. Similarly, Jahn-Teller distortion in the pseudo octahedral complex (1) can lead to elongation (z-out) or to compression (z-in) of a pair of opposite Ni-N bonds, see Fig. 2.

As was found for (2) and (3), the longest terminal bonds (2.105 Å) of (1) are also ca 0.18 Å longer than the average other four Ni(III)-N bonds, that could be interpreted that as (1) also having elongation Jahn-Teller distortion with the elongated bonds the two longest terminal bonds (2.105 Å). This agree with the fact that the 1.977 Å terminal bonds are nearer in length to the average of the shorter central constrained bonds of 1.865 Å (only 0.111 Å longer) than to the 2.105 Å longest terminal bonds (0.128 Å shorter). Compared to the Ni(II)-N bonds in the related polypyridine-nickel(II) complexes, the elongated Ni(III)-N bonds in (1) – (3) in the z-direction, changed slightly in length (up to 0.06 Å, most pronounced for (2) and (3)). However, the four shorter Ni(III)-N bonds in the equatorial plane are significantly shorter than the Ni(II)-N bonds, more than 0.13, 0.12 and 0.14 Å for (1) – (3) respectively (see  $\Delta d$  values in Table 1). The change in the bond lengths are further validation that (1) also exhibit elongation Jahn-Teller distortion. Compared to (2) and (3), the elongated Ni(III)-N bonds in (1) are slightly shorter; ca 2.11 Å in (1) versus 2.13 and 2.15 in (2) and (3) respectively. The four Ni(III)-N bonds of (1) in the xy-plane (1.977, 1.977, 1.882 and 1.848 Å), are similar in length to the Ni(III)-N bonds of (2) (1.950 and 1.946) and (3) (1.961 and 1.949) in the xy-plane. Thus the elongated bonds in (1) – (3) are longer than 2.1 Å and the bonds in the xy-plane are all less than 2 Å.

The OLYP-D3/ZORA-TZ2P optimized geometry of (1), with two long

**Table 1**

DFT gas phase calculated Ni-N bond lengths (Å) of optimized geometries of polypyridine-nickel(III) complexes (1) – (3) and related polypyridine-nickel(II) complexes using the indicated DFT method. The optimized geometries of (1) as obtained by different DFT methods are indicated as (1a) – (1f).

No	DFT method		Ni-N <sub>z</sub>	Ni-N <sub>xy1</sub>	Ni-N <sub>xy2</sub>	Jahn-Teller
2	OLYP-D3/ZORA-TZ2P 	[Ni(bpy) <sub>3</sub> ] <sup>3+</sup>	2.130	1.950	1.946	elongation
		[Ni(bpy) <sub>3</sub> ] <sup>2+</sup>	2.074	2.074	2.074	–
		Δd <sup>a</sup>	0.056	–0.124	–0.128	
		Δx <sup>b</sup>	0.181		0.003	
3	OLYP-D3/ZORA-TZ2P 	[Ni(phen) <sub>3</sub> ] <sup>3+</sup>	2.148	1.961	1.949	elongation
		[Ni(phen) <sub>3</sub> ] <sup>2+</sup>	2.100	2.100	2.100	–
		Δd <sup>a</sup>	0.048	–0.140	–0.151	
		Δx <sup>b</sup>	0.188		0.012	
1a	OLYP-D3/ZORA-TZ2P 	[Ni(tpy) <sub>z</sub> ] <sup>3+</sup>	Ni-N <sub>terminal1</sub> <sup>d</sup> 2.105	Ni-N <sub>terminal2</sub> 1.977	Ni-N <sub>central(average)</sub> 1.865	Jahn-Teller elongation
		[Ni(tpy) <sub>z</sub> ] <sup>2+</sup>	2.103	2.103	1.996	–
		Δd <sup>a</sup>	0.001	–0.127	–0.131	
		Δx <sup>b</sup>	0.128		<b>0.111</b>	
1b	OLYP-D3/ZORA-TZ2P	[Ni(tpy) <sub>z</sub> ] <sup>3+ e</sup>	2.114	2.021	1.875	compression
		[Ni(tpy) <sub>z</sub> ] <sup>2+</sup>	2.103	2.103	1.996	–
		Δd <sup>a</sup>	0.011	–0.083	–0.121	
		Δx <sup>b</sup>	<b>0.093</b>		0.145	
1c	OLYP/ZORA-TZ2P	[Ni(tpy) <sub>z</sub> ] <sup>3+</sup>	2.132	2.072	1.885	compression
		[Ni(tpy) <sub>z</sub> ] <sup>2+</sup>	2.155	2.155	2.010	–
		Δd <sup>a</sup>	–0.023	–0.083	–0.125	
		Δx <sup>b</sup>	<b>0.060</b>		0.187	
1d	OLYP-D3/6-311G(d,p)	[Ni(tpy) <sub>z</sub> ] <sup>3+</sup>	2.114	2.021	1.875	compression
		[Ni(tpy) <sub>z</sub> ] <sup>2+</sup>	2.124	2.124	1.995	–
		Δd <sup>a</sup>	–0.010	–0.104	–0.119	
		Δx <sup>b</sup>	<b>0.093</b>		0.145	
1e	OLYP-D3/6-311G(d,p)	[Ni(tpy) <sub>z</sub> ] <sup>3+ f</sup>	2.105	1.977	1.865	elongation
		[Ni(tpy) <sub>z</sub> ] <sup>2+</sup>	2.124	2.124	1.995	–
		Δd <sup>a</sup>	–0.020	–0.148	–0.129	
		Δx <sup>b</sup>	0.128		<b>0.111</b>	
1f	OLYP/6-311G(d,p)	[Ni(tpy) <sub>z</sub> ] <sup>3+</sup>	2.119	2.070	1.886	compression
		[Ni(tpy) <sub>z</sub> ] <sup>2+</sup>	2.154	2.154	2.011	–
		Δd <sup>a</sup>	–0.035	–0.085	–0.125	
		Δx <sup>b</sup>	<b>0.050</b>		0.184	

a Δd is the change in bond length d(Ni(III)-N) – d(Ni(II)-N) in Å.

b Δx is the difference in bond length of the Ni(III)-N bond of medium length (Ni(III)-N<sub>terminal2</sub> or Ni(III)-N<sub>xy1</sub>) from the longest (Ni(III)-N<sub>terminal1</sub> or Ni(III)-N<sub>y</sub>) and from the shortest (Ni(III)-N<sub>central</sub> or Ni(III)-N<sub>xy2</sub>) bond for (1) – (3), in Å.

d For [Ni(tpy)<sub>z</sub>]<sup>3+</sup> Ni-N<sub>terminal1</sub> is chosen as the longer pair of bonds.

e Single point (sp) using OLYP-D3/6-311G(d,p) compression optimized geometry 1d.

f Single point (sp) using OLYP-D3/Z-TZ2P elongation optimized geometry 1a.

(2.105 Å), two medium (1.977 Å) and two short (1.865 Å) Ni(III)-N bonds, can thus be described as elongation Jahn-Teller distortion, similar to orthorhombic elongation Jahn-Teller distortion in orthorhombic distorted octahedral complexes [18,43].

#### Mulliken spin density and frontier orbitals

Since the spin of the d<sup>7</sup> tris(polypyridine)nickel(III) complexes (2) and (3) is ½, the spin density plots of (2) and (3) show the locus of the unpaired electron in the e<sub>g</sub> orbital set, see Fig. 3. The spin density plots of (2) and (3) clearly show that the unpaired electron in the e<sub>g</sub> orbital set has d<sub>z<sup>2</sup></sub> character, consistent with elongation Jahn-Teller distortion. The unpaired electron resides in the highest occupied molecular orbital (HOMO) of (2) and (3), with similar d<sub>z<sup>2</sup></sub> character, see Fig. 3. The lowest unoccupied molecular orbital (LUMO) of (2) and (3) exhibits similar d<sub>x<sup>2</sup>-y<sup>2</sup></sub> character, see Fig. 3.

The observed elongation of the Ni(III)-N bonds along the z-axis is

dictated by the anti-bonding interaction between the d<sub>z<sup>2</sup></sub> MO on Ni and the p<sub>z</sub> MOs on the N's involved, leading to elongation of the Ni(III)-N bonds along the z-axis. The elongation Jahn-Teller distortion lowers the overall energy of the system. This distortion is driven by the interaction between electronic and vibrational degrees of freedom, which is referred to as vibronic coupling. The electronic energy levels and the vibrational energy levels become coupled or correlated [45]. Vibronic interaction has the effect of further lowering the energy of the distorted system, leading to the lowering of the energy of the d<sub>z<sup>2</sup></sub> HOMO and raising the energy of the d<sub>x<sup>2</sup>-y<sup>2</sup></sub> (LUMO) (MO energies are given in Fig. 3).

The Mulliken spin density plot of (1) have very similar character as the spin plots of (2) and (3) (Fig. 3). The Mulliken spin density on Ni of (1) is slightly lower than that of (2) and (3), namely 0.618, 0.641 and 0.648 e<sup>–</sup>, for (1) – (3) respectively, see data in Table 2 (OLYP-D3/ZORA-TZ2P data of 1 is indicated under optimized geometry 1a in Table 2).

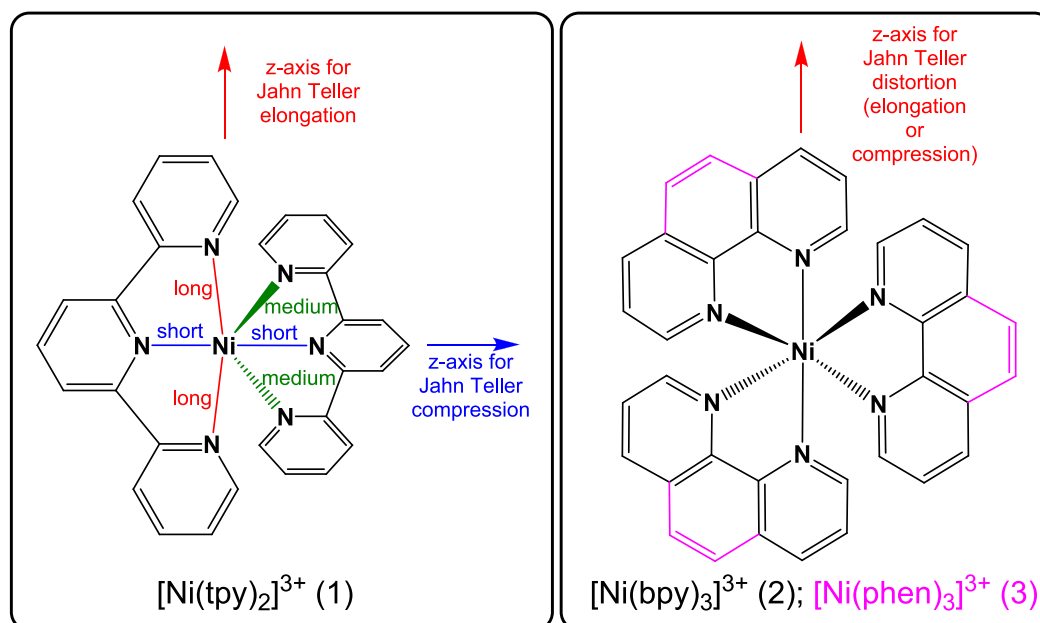


Fig. 2. Jahn-Teller distortion in (1), (2) and (3), leading to elongation (z-out) or compression (z-in) of a pair of opposite bonds along the indicated z-axis direction.

The Mulliken spin density of molecule (1, geometry 1a) on the N's along the longer z-axis (0.135  $e^-$  on both N's) is much larger (greater than 0.09  $e^-$ ) than the spin density on the N's of the shorter bonds equatorial bonds in the xy-plane (0.043, 0.043, 0.011 and  $-0.006 e^-$  respectively, or an average of 0.023  $e^-$ ). For (2) and (3) the N's in the xy-plane,  $N_x$  and  $N_y$ , all have a spin density of 0.016  $e^-$ , slightly lower than the spin density of some of the N's in the xy-plane of (1) (up to 0.043  $e^-$ ).

The HOMO and LUMO of (1) in Fig. 3, have very similar character as the HOMOs and LUMOs of (2) and (3). All HOMOs look very similar with ca 40% Ni-d character, ca 30% on  $N_z$ , and a small amount (up to 10%) on  $N_y$  and  $N_x$ .  $N_z$  is the N on the z-axis as defined in Fig. 3, similar for  $N_x$  and  $N_y$ .

The similar character of the spin plot, HOMO and LUMO of (1) compared to that of (2) and (3), see Fig. 3, is consistent with (1) having elongation Jahn-Teller distortion, like (2) and (3).

#### Jahn Teller elongation and compression optimized geometries of (1)

In this section the optimized geometries and observed Jahn-Teller distortion, the spin density profile and important molecular orbitals (MOs) of (1), obtained using different DFT methods, are discussed. The results show, that depending on the DFT method, different optimized structures of (1), numbered geometry 1a – 1f, are obtained (Table 1).

#### Geometry and energy

The strain of the tridentate terpyridine ligand in (1) could lead to elongation Jahn-Teller distortion, Fig. 2. However, compression Jahn-Teller distortion is experimentally observed for high spin  $d^4$  bis(terpyridine)manganese(III) [46] and low spin  $d^7$  tris(bipyridine)nickel(III) [35]. Although the OLYP-D3/ZORA-TZ2P DFT method reproduced experimental Ni(II)-N terminal and central bonds of bis(terpyridine)nickel(II) most accurately (within 0.008 Å), no DFT calculated compression Jahn-Teller geometries without an imaginary frequency, could be optimized for (1) – (3) when using the OLYP-D3/ZORA-TZ2P DFT method.

A compression Jahn-Teller distortion geometry for (1) was obtained, using the OLYP/ZORA-TZ2P method, thus with the OLYP functional without D3 dispersion, with terminal bond lengths of 2.132 and 2.072 Å and central compressed bonds of 1.885 Å (See geometry 1c in Table 1). Compared to the related OLYP/ZORA-TZ2P bis(terpyridine)nickel(II)

complex, all the Ni(III)-N bonds geometry 1c are shorter. The central compressed Ni(III)-N bonds, and the terminal bonds are shorter by 0.125, 0.023 and 0.083 Å respectively (see  $\Delta d$  values in Table 1). The terminal Ni(III)-N bonds of medium length (2.072 Å,  $\text{Ni-N}_{\text{terminal2}}$  in Table 1), are nearer in length to the 2.132 Å longest terminal bonds (0.060 Å shorter) than to the average of the shorter central constrained bonds of 1.885 Å (0.187 Å longer), ( $\Delta x$  values in Table 1). The bond lengths of geometry 1c are consistent with the OLYP/ZORA-TZ2P calculated geometry of (1) exhibiting compression Jahn-Teller distortion, with the z-axis now defined along the central bonds (Fig. 2).

The OLYP-D3/6-311G(d,p) method, in contrary to the OLYP-D3/ZORA-TZ2P method, produced a compression Jahn-Teller distortion geometry for (1), see bond length values of the compression geometry 1d in Table 1. Using the OLYP-D3/Z-TZ2P method on the optimized coordinates of this compression OLYP-D3/6-311G(d,p) geometry 1d (single point calculation, producing compression geometry 1b), energies and spin populations could be obtained to be compared to the elongation optimized OLYP-D3/ZORA-TZ2P geometry 1a, see values in Table 1 and Table 2. This single point calculation did not have any imaginary frequency, and compression geometry 1b was only 0.018 eV higher in electronic energy than the elongation optimized OLYP-D3/ZORA-TZ2P structure, geometry 1a. However, the free energy of compression geometry 1b is 0.005 eV lower than the free energy of elongation geometry 1a (see energies in Table 3). The population of elongation geometry 1a (45.2%) and compression geometry 1b (54.8%), obtained by using the Boltzmann equation, are very similar, implying both the elongation and compression geometries of (1) are possible. The small difference in energy between the optimized elongation geometry 1a and sp compression geometry 1b, may be the reason why, when re-optimizing the compression OLYP-D3/6-311G(d,p) geometry 1d, using the OLYP-D3/Z-TZ2P method, the compression input geometry converged to an elongation geometry (1a in Table 1).

Since the OLYP-D3/6-311G(d,p) method, produced a compression Jahn-Teller distortion geometry for (1), geometry 1d in Table 1 and Fig. S1 in the supporting information, a single point calculation (elongation geometry 1e) using the optimized coordinates of the elongation optimized OLYP-D3/ZORA-TZ2P geometry 1a was done to get OLYP-D3/6-311G(d,p) energies to be compared to the values of geometry 1d. The minimum energy OLYP-D3/6-311G(d,p) compression geometry 1d was only 0.035 eV lower in electronic and 0.048 eV in free energy

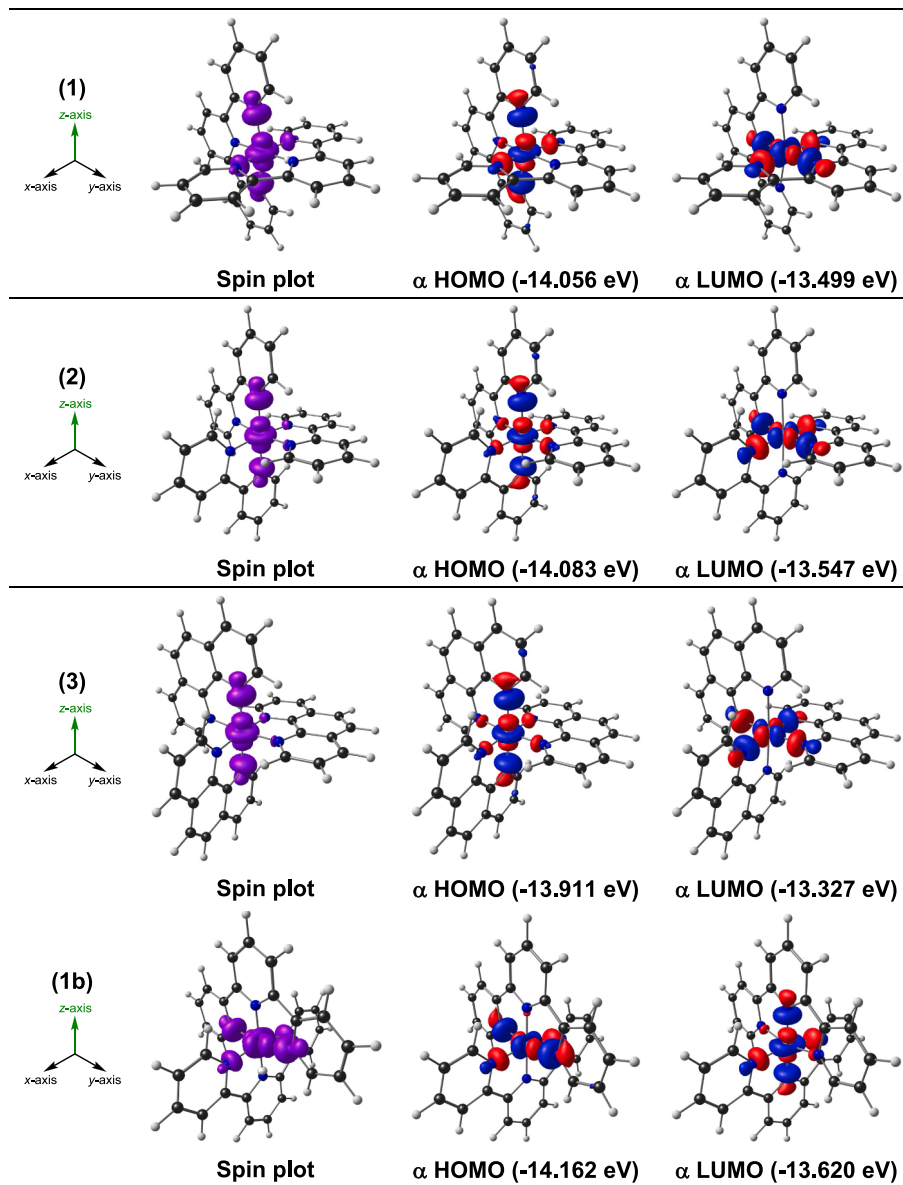


**Fig. 3.** Spin plots, frontier orbitals and MO energies of the OLYP-D3/ZORA-TZ2P gas phase optimized geometries of polypyridine-nickel(III) complexes (1) – (3). Color scheme used for atoms (online version): Ni (purple), N (blue), C (black) and H (white). Contours of 0.004 and 0.06  $\text{e}\text{\AA}^{-3}$  are used for the spin and MO plots respectively. (For interpretation of the references to color in this figure legend, the reader is referred to the web version of this article.)

than the OLYP-D3/6-311G(d,p) single point elongation geometry 1e (no imaginary frequency). The population obtained for the OLYP-D3/6-311G(d,p) calculated elongation geometry 1e (13.2%) and compression geometry 1d (86.8%) (Table 3), differ slightly from the population when using the OLYP-D3/Z-TZ2P method (45.2% for compression and 54.8% for elongation), though both methods predict that both the compression and elongation geometries are energetically possible (see energies in Table 3).

The OLYP/6-311G(d,p) method (OLYP functional without D3 dispersion) also produced a compression Jahn-Teller distortion geometry for (1), geometry 1f in Table 1.

The results obtained thus indicate that both the elongation and compression geometries of (1) are possible, and with favourable experimental conditions, both geometries should be experimentally isolated.

#### Mulliken spin density and frontier MOs of (1)

Mulliken spin populations, the %Ni-d and %N character and energies

of the HOMO and LUMO of (1) – (3), obtained by the different DFT methods as mentioned in Table 1, are summarized in Table 2.

The spin plot of the OLYP-D3/ZORA-TZ2P elongation optimized geometry of (1), geometry 1a, (Fig. 3), is of the  $d_{z^2}$  character ( $0.618 e^-$ ) with some spin density on the  $N_z$  atoms ( $0.135 e^-$ ) of  $p_z$  character. In addition, a smaller amount of spin density ( $0.043 e^-$ ) is visible on the  $N_x$  atoms of  $p_x$  character. The HOMO looks very similar to the spin density plot, residing 41.8% on Ni, 30.4% on  $N_z$ , 1% on  $N_y$  and 10.4% on  $N_x$  ( $N_z$  is the N on the z-axis along the central bonds). The LUMO resides 46.2% on Ni- $d_{x^2-y^2}$ , 12.0% on  $N_y$  and 17.2% on  $N_x$ .

In contrary, the spin plot of the OLYP/ZORA-TZ2P compression calculated geometry of (1), geometry 1c, show that the locus of the unpaired electron in the  $e_g$  orbital set is of  $d_{x^2-y^2}$  character (Fig. S1 in the supporting information), consistent with compression Jahn-Teller distortion (Fig. 1). In this compression optimized molecule,  $0.640 e^-$  of the spin density is on Ni,  $0.069 e^-$  on  $N_x$  and  $0.108 e^-$  on  $N_y$ . The unpaired electron resides in the singly occupied molecular orbital (SOMO that is the HOMO) of geometry 1c, with similar  $d_{x^2-y^2}$  character,

**Table 2**

DFT gas phase calculated energy and composition of the HOMO and LUMO and Mulliken spin densities (average values) of optimized the geometries of bis(terpyridine)nickel(III) complex (1, point group  $C_{2v}$ ), tris(bipyridine)nickel(III) (2, point group  $C_2$ ) and tris(phenanthroline)nickel(III) (3, point group  $C_2$ ), using the indicated DFT method. HOMOs, LUMOs and Mulliken spin density plots of (1) are visualized in Fig. S1 in the supporting information.  $N_z$  is the N on the z-axis as defined in Fig. 3, similar for  $N_x$  and  $N_y$ .

Optimized geometry	DFT method	MO	MO composition (%)				MO energy E (eV)	Spin density ( $e^-$ )				Jahn-Teller
			%d Ni	%p $N_z$	%p $N_y$	%p $N_x$		Ni	$N_z$	$N_y$	$N_x$	
1a	OLYP-D3/ZORA-TZ2P	HOMO	41.8	30.4	1.0	10.4	-14.056	0.618	0.135	0.003	0.043	elongation
		LUMO	46.2	1.1	12.0	17.2	-13.499					
2	OLYP-D3/ZORA-TZ2P	HOMO	42.3	31.1	5.1	5.1	-14.083	0.641	0.136	0.016	0.016	elongation
		LUMO	45.5	0.0	27.8	27.8	-13.547					
3	OLYP-D3/ZORA-TZ2P	HOMO	40.0	30.2	0.0	4.7	-13.911	0.648	0.133	0.016	0.016	elongation
		LUMO	45.8	0.0	20.2	20.2	-13.327					
1b <sup>a</sup>	OLYP-D3/ZORA-TZ2P	HOMO	41.6	0.0	13.4	28.2	-14.162	0.630	-0.005	0.057	0.122	compression
		LUMO	46.1	12.4	14.4	2.4	-13.620					
1c	OLYP/ZORA-TZ2P	HOMO	40.4	0.0	17.3	25.8	-14.301	0.640	-0.009	0.069	0.108	compression
		LUMO	45.3	12.4	12.0	3.9	-13.750					
1d	OLYP-D3/6-311G(d,p)	HOMO	42.8	0.0	6.8	13.4	-13.932	0.679	-0.013	0.052	0.118	compression
		LUMO	47.2	10.5	6.6	1.3	-13.415					
1e <sup>b</sup>	OLYP-D3/6-311G(d,p)	HOMO	43.0	14.4	1.6	5.3	-13.823	0.667	0.131	-0.005	0.038	elongation
		LUMO	47.3	1.4	10.1	6.5	-13.279					
1f	OLYP/6-311G(d,p)	HOMO	42.4	0.0	8.6	12.0	-14.041	0.690	-0.017	0.067	0.101	compression
		LUMO	46.9	11.6	4.4	2.2	-13.524					

a Single point (sp) using OLYP-D3/6-311G(d,p) compression optimized geometry 1d.

b Single point (sp) using OLYP-D3/Z-TZ2P elongation optimized geometry 1a.

**Table 3**

DFT gas phase calculated electronic energies (E in eV), free energies (G in eV) and population (%) at 1 atm and 298.15 K) of optimized geometries of bis(terpyridine)nickel(III) complex (1, point group  $C_{2v}$ ), using the indicated DFT method.

Optimized geometry	DFT method	$\Delta E$	$\Delta G$	% Population	Jahn-Teller
1a	OLYP-D3/Z-TZ2P	0.000	0.005	45.2	elongation
1b	OLYP-D3/Z-TZ2P	0.018	0.000	54.8	compression
1d	OLYP-D3/6-311G(d,p)	0.000	0.000	86.8	compression
1e	OLYP-D3/6-311G(d,p)	0.035	0.048	13.2	elongation

see Fig. S1 in the supporting information. The HOMO has 40.4% Ni-d character, with 17.3% on  $N_y$  and 25.8% on  $N_x$ . The lowest unoccupied molecular orbital (LUMO) or the singly unoccupied molecular orbital (SUMO) of the  $S = \frac{1}{2}$  OLYP/ZORA-TZ2P calculated geometry 1c of (1) exhibits  $d_{z^2}$  character. The spin density plots, HOMOs and LUMOs of the other compression geometries shown Fig. S1 in the supporting information, are similar to the OLYP/ZORA-TZ2P compression calculated geometry of (1), geometry 1c. The Mulliken spin on  $N_x$  and  $N_y$  of the compression geometries are less than the Mulliken spin on  $N_z$  of the elongation geometries, though observable more than the small amount of spin on  $N_x$  of the compression geometries. For both the compression and elongation geometries, the LUMO has nearly 5% more d character than the HOMO.

#### Distinguishing between a elongation and compression geometry for (1)

Due to the strain in the central Ni-N bond of bis(terpyridine)nickel(III), complex (1), the central Ni-N bond are always shorter than the terminal Ni-N bonds. Distinguishing between a elongation and compression geometry for (1), thus seems to be very subtle. The following criteria can be used:

- If the difference in bond length of Ni(III)- $N_{\text{terminal}2}$  and Ni(III)- $N_{\text{terminal}1}$  is smaller than the difference in bond length of Ni(III)- $N_{\text{terminal}2}$  and Ni(III)- $N_{\text{central}}$  ( $\Delta x$  in Table 1), then it is a Jahn-

Teller compression geometry (and vice versa for a Jahn-Teller elongation geometry).

- The change in both the Ni- $N_{\text{terminal}2}$  and Ni- $N_{\text{central}}$  bond lengths upon reduction of Ni(III),  $\Delta d$  in Table 1, are more significant (ca 0.13 Å or more) for the Jahn-Teller elongation geometry, than for the compression geometry. For a compression geometry the change in the Ni- $N_{\text{terminal}2}$  and Ni- $N_{\text{central}}$  bond lengths are ca 0.08 and 0.12 Å respectively.
- The character of the spin density plot is  $d_{x^2-y^2}$  for a Jahn-Teller compression geometry (z-direction along the central bonds) and  $d_{z^2}$  for elongation (z-direction along the longest terminal bonds).
- The character of the SOMO and SUMO is  $d_{x^2-y^2}$  and  $d_{z^2}$  respectively for a Jahn-Teller compression (z-direction along the central bonds), and vice versa for elongation (z-direction along the longest terminal bonds).
- Significant Mulliken spin population on both  $N_x$  and  $N_y$  (near zero on  $N_z$ ) for a Jahn-Teller compression (z-direction along the central bonds). Significant Mulliken spin population on  $N_z$  (near zero or small on  $N_x$  and  $N_y$ ) for elongation (z-direction along the longest terminal bonds).

#### Conclusions

The OLYP-D3/ZORA-TZ2P DFT method reproduced experimental Ni(II)-N terminal and central bonds of bis(terpyridine)nickel(II) most accurately within 0.008 Å. The results obtained indicate that both the elongation and compression geometries of (1) are possible, and with favourable experimental conditions, should be experimentally isolated. However, the strain of the tridentate terpyridine ligand in bis(terpyridine)nickel(III) complicates the identification of the type of Jahn-Teller distortion observed. A set of criteria were identified that can be used in the identification of the type of Jahn-Teller distortion. The easiest criteria to apply is, to determine the bond length differences (Ni(III)- $N_{\text{terminal}1}$  - Ni(III)- $N_{\text{terminal}2}$ ) and (Ni(III)- $N_{\text{terminal}2}$  - Ni(III)- $N_{\text{central}}$ ), where Ni(III)- $N_{\text{terminal}1}$  is the longest pair of bonds. If the value of (Ni(III)- $N_{\text{terminal}1}$  and Ni(III)- $N_{\text{terminal}2}$ ) is smaller than (Ni(III)- $N_{\text{terminal}2}$  - Ni(III)- $N_{\text{central}}$ ), then it is a Jahn-Teller compression geometry (and vice versa for a Jahn-Teller elongation geometry).

#### CRediT authorship contribution statement

Jeanet Conradie: Conceptualization, Methodology, Writing –

review & editing.

## Declaration of Competing Interest

The authors declare that they have no known competing financial interests or personal relationships that could have appeared to influence the work reported in this paper.

## Data availability

Data within article and [supporting information](#).

## Acknowledgements

“This work has received support the South African National Research Foundation (NRF, grant numbers 129270 and 132504) and the Central Research Fund (CRF) of the University of the Free State (UFS), Bloemfontein, RSA. The High-Performance Computing (HPC) facility of the UFS, the NICIS CSIR Centre for High Performance Computing (CHPC, grant CHEM0947) of RSA and the Norwegian Supercomputing Program (UNINETT Sigma2, Grant No. NN9684K) are acknowledged for computer time.”

## Appendix A. Supplementary data

Figure S1 and optimized coordinates of the DFT calculations. Supplementary data to this article can be found online at <https://doi.org/10.1016/j.rechem.2023.101191>.

## References

- Y. Budnikova, D. Vicić, A. Klein, Exploring Mechanisms in Ni Terpyridine Catalyzed C-C Cross-Coupling Reactions—A Review, *Inorganics*. 6 (2018) 18, <https://doi.org/10.3390/inorganics6010018>.
- N. Elgrishi, M.B. Chambers, V. Artero, M. Fontecave, Terpyridine complexes of first row transition metals and electrochemical reduction of CO<sub>2</sub> to CO, *Phys. Chem. Chem. Phys.* 16 (2014) 13635–13644, <https://doi.org/10.1039/C4CP00451E>.
- C. Arana, S. Yan, M. Keshavarz-K, K.T. Potts, H.D. Abruna, Electrochemical reduction of carbon dioxide with iron, cobalt, and nickel complexes of terdentate ligands, *Inorg. Chem.* 31 (1992) 3680–3682, <https://doi.org/10.1021/ic00043a034>.
- A. Juneja, T.S. Macedo, D.R. Magalhães Moreira, M.B. Pereira Soares, A.C. Lima Leite, J. Kelle de Andrade Lemoine Neves, V.R. Alves Pereira, F. Avevilla, A. Azam, Synthesis of 4'-(2-ferrocenyl)-2,2':6'2"-terpyridine: Characterization and antiproteoal activity of Mn(II), Co(II), Ni(II), Cu(II) and Zn(II) complexes, *Eur. J. Med. Chem.* 75 (2014) 203–210. [10.1016/j.ejmech.2014.01.051](https://doi.org/10.1016/j.ejmech.2014.01.051).
- C. Mugemana, P. Guillet, S. Hoepfner, U.S. Schubert, C.-A. Fustin, J.-F. Gohy, Metallo-supramolecular diblock copolymers based on heteroleptic cobalt(III) and nickel(II) bis-terpyridine complexes, *Chem. Commun.* 46 (2010) 1296, <https://doi.org/10.1039/b923270b>.
- B.Z. Momeni, F. Rahimi, S.M. Jebraeil, J. Janczak, Supramolecular structures of Ni (II) and Pt(II) based on the substituted 2, 2': 6', 6'2"-terpyridine: Synthesis, structural characterization, luminescence and thermal properties, *J. Mol. Struct.* 1150 (2017) 196–205, <https://doi.org/10.1016/j.molstruc.2017.08.081>.
- B.Z. Momeni, S.K. Anari, M. Torrei, J. Janczak, Crystal exploring, Hirshfeld surface analysis, and properties of 4'-(furan-2-yl)-2,2':6',2"-terpyridine complexes of nickel (II): New precursors for the synthesis of nanoparticles, *Appl. Organomet. Chem.* 35 (2021) 1–22, <https://doi.org/10.1002/aoc.6179>.
- C.R. Groom, I.J. Bruno, M.P. Lightfoot, S.C. Ward, The Cambridge Structural Database, *Acta Crystallogr. Sect. B Struct. Sci. Cryst. Eng. Mater.* 72 (2016) 171–179, <https://doi.org/10.1107/S2052520616003954>.
- A.G. Orpen, Applications of the Cambridge Structural Database to molecular inorganic chemistry, *Acta Crystallogr. Sect. B Struct. Sci.* 58 (2002) 398–406, <https://doi.org/10.1107/S01087681020004895>.
- F.H. Allen, W.D.S. Motherwell, Applications of the Cambridge Structural Database in organic chemistry and crystal chemistry, *Acta Crystallogr. Sect. B Struct. Sci.* 58 (2002) 407–422, <https://doi.org/10.1107/S01087681020004895>.
- J.R. Jeitler, M.M. Turnbull, J.L. Wikaira, Synthesis, characterization and structure of transition metal complexes of 4'-methylthio-2,2': 6',2"-terpyridyl, *Inorganica Chim. Acta.* 351 (2003) 331–334, [https://doi.org/10.1016/S0020-1693\(03\)00175-0](https://doi.org/10.1016/S0020-1693(03)00175-0).
- C. Alonso, L. Ballester, A. Gutiérrez, M.F. Perpiñán, A.E. Sánchez, M.T. Azcondo, Tetracyanoquinodimethanido Derivatives of (Terpyridine)- and (Phenanthroline) metal Complexes - Structural and Magnetic Studies of Radical-Ion Salts, *Eur. J. Inorg. Chem.* 2005 (2005) 486–495, <https://doi.org/10.1002/ejic.200400540>.
- R. Freitag, J. Conradie, Understanding the Jahn-Teller Effect in Octahedral Transition-Metal Complexes: A Molecular Orbital View of the Mn(β-diketonato)3 Complex, *J. Chem. Educ.* 90 (2013) 1692–1696, <https://doi.org/10.1021/ed400370p>.
- J. Conradie, Jahn-Teller effect in high spin d4 and d9 octahedral metal-complexes, *Inorganica Chim. Acta.* 486 (2019) 193–199, <https://doi.org/10.1016/j.ica.2018.10.040>.
- H.A. Jahn, E. Teller, Stability of polyatomic molecules in degenerate electronic states - I—Orbital degeneracy, *Proc. R. Soc. London. Ser. A - Math. Phys. Sci.* 161 (1937) 220–235. [10.1098/rspa.1937.0142](https://doi.org/10.1098/rspa.1937.0142).
- J.C. Dickenson, M.E. Haley, J.T. Hyde, Z.M. Reid, T.J. Tarring, D.A. Iovan, D. P. Harrison, Fine-Tuning Metal and Ligand-Centered Redox Potentials of Homoleptic Bis-Terpyridine Complexes with 4'-Aryl Substituents, *Inorg. Chem.* 60 (2021) 9956–9969, <https://doi.org/10.1021/acs.inorgchem.1c01233>.
- M. Wang, J. England, T. Weyhermüller, K. Wieghardt, Electronic structures of “low-valent” neutral complexes [NiL<sub>2</sub>]O (S = 0; L = bpy, phen, tpy) - An experimental and DFT computational study, *Eur. J. Inorg. Chem.* 2015 (2015) 1511–1523, <https://doi.org/10.1002/ejic.201403144>.
- S. Geremia, N. Demitri, Crystallographic Study of Manganese(III) Acetylacetonate: An Advanced Undergraduate Project with Unexpected Challenges, *J. Chem. Educ.* 82 (2005) 460, <https://doi.org/10.1021/ed082p460>.
- A. Davidson, J.F. Tempere, M. Che, H. Roulet, G. Dufour, Spectroscopic studies of nickel(II) and nickel(III) species generated upon thermal treatments of nickel/ceria-supported materials, *J. Phys. Chem.* 100 (1996) 4919–4929, <https://doi.org/10.1021/jp952268w>.
- D.-Y. Noh, J.-H. Choy, Magnetic properties of nickel(III) bis(benzene-1,2-dithiolate); (n-Bu<sub>4</sub>N)[Ni(dmbit)<sub>2</sub>] and (n-Bu<sub>4</sub>N)[Ni(dmbip)<sub>2</sub>], *Synth. Met.* 70 (1995) 1059–1060, [https://doi.org/10.1016/0379-6779\(94\)02757-P](https://doi.org/10.1016/0379-6779(94)02757-P).
- P.-F. Wang, T. Jin, J. Zhang, Q.-C. Wang, X. Ji, C. Cui, N. Piao, S. Liu, J. Xu, X.-Q. Yang, C. Wang, Elucidation of the Jahn-Teller effect in a pair of sodium isomer, *Nano Energy.* 77 (2020), 105167, <https://doi.org/10.1016/j.nanoen.2020.105167>.
- C.R. Dennis, D.W. Margerum, E. Fourie, J.C. Swarts, A Kinetic Study of the Electron-Transfer Reactions of Nickel(III, II) Tripeptide Complexes with Cyano Complexes of Molybdenum, Tungsten, and Iron, *Inorg. Chem.* 59 (2020) 11695–11703, <https://doi.org/10.1021/acs.inorgchem.0c01582>.
- Chemcraft - graphical software for visualization of quantum chemistry computations., (n.d.). <http://www.chemcraftprog.com/>.
- N.C. Handy, A.J. Cohen, Left-right correlation energy, *Mol. Phys.* 99 (2001) 403–412, <https://doi.org/10.1080/00268970010018431>.
- C. Lee, W. Yang, R.G. Parr, Development of the Colle-Salvetti correlation-energy formula into a functional of the electron density, *Phys. Rev. B* 37 (1988) 785–789, <https://doi.org/10.1103/PhysRevB.37.785>.
- S. Grimme, J. Antony, S. Ehrlich, H. Krieg, A consistent and accurate ab initio parametrization of density functional dispersion correction (DFT-D) for the 94 elements H-Pu, *J. Chem. Phys.* 132 (2010), 154104, <https://doi.org/10.1063/1.3382344>.
- J. Conradie, T. Wondimagegn, A. Ghosh, Spin States at a Tipping Point: What Determines the dz<sub>2</sub> Ground State of Nickel(III) Tetra(tbutyl)porphyrin Dicyanide? *J. Phys. Chem. B.* 112 (2008) 1053–1056, <https://doi.org/10.1021/jp709980y>.
- E. van Lenthe, E.J. Baerends, J.G. Snijders, Relativistic total energy using regular approximations, *J. Chem. Phys.* 101 (1994) 9783–9792, <https://doi.org/10.1063/1.467943>.
- E. van Lenthe, A. Ehlers, E.-J. Baerends, Geometry optimizations in the zero order regular approximation for relativistic effects, *J. Chem. Phys.* 110 (1999) 8943–8953, <https://doi.org/10.1063/1.478813>.
- E. van Lenthe, E.J. Baerends, J.G. Snijders, Relativistic regular two-component Hamiltonians, *J. Chem. Phys.* 99 (1993) 4597–4610, <https://doi.org/10.1063/1.466059>.
- G. te Velde, F.M. Bickelhaupt, E.J. Baerends, C. Fonseca Guerra, S.J.A. van Gisbergen, J.G. Snijders, T. Ziegler, Chemistry with ADF, *J. Comput. Chem.* 22 (2001) 931–967, <https://doi.org/10.1002/jcc.1056>.
- C. Fonseca Guerra, J.G. Snijders, G. te Velde, E.J. Baerends, Towards an order-N DFT method, *Theor. Chem. Accounts Theory, Comput. Model. (Theoretica Chim. Acta).* 99 (1998) 391–403, <https://doi.org/10.1007/s002140050353>.
- M.J. Frisch, G.W. Trucks, H.B. Schlegel, G.E. Scuseria, M.A. Robb, J.R. Cheeseman, G. Scalmani, V. Barone, G.A. Petersson, H. Nakatsuji, X. Li, M. Caricato, A. V. Marenich, J. Bloino, B.G. Janesko, R. Gomperts, B. Mennucci, H.P. Hratchian, J. V. Ortiz, A.F. Izmaylov, J.L. Sonnenberg, D. Williams-Young, F. Ding, F. Lipparini, F. Egidi, J. Goings, B. Peng, A. Petrone, T. Henderson, D. Ranasinghe, V.G. Zakrzewski, J. Gao, N. Rega, G. Zheng, W. Liang, M. Hada, M. Ehara, K. Toyota, R. Fukuda, J. Hasegawa, M. Ishida, T. Nakajima, Y. Honda, O. Kitao, H. Nakai, T. Vreven, K. Throssell, J. Montgomery, J. A., J.E. Peralta, F. Ogliaro, M.J. Bearpark, J.J. Heyd, E.N. Brothers, K.N. Kudin, V.N. Staroverov, T.A. Keith, R. Kobayashi, J. Normand, K. Raghavachari, A.P. Rendell, J.C. Burant, S.S. Iyengar, J. Tomasi, M. Cossi, J.M. Millam, M. Klene, C. Adamo, R. Cammi, J.W. Ochterski, R.L. Martin, K. Morokuma, O. Farkas, J.B. Foresman, D.J. Fox, Gaussian 16, Revision B.01, (2016).
- H. Hadadzadeh, G. Mansouri, A. Rezvani, H.R. Khavasi, B.W. Skelton, M. Makha, F. R. Charati, Mononuclear nickel(II) complexes coordinated by polypyridyl ligands, *Polyhedron.* 30 (2011) 2535–2543, <https://doi.org/10.1016/j.poly.2011.06.037>.
- D.J. Szalda, D.H. Macartney, N. Sutin, Electron-transfer barriers and metal-ligand bonding as a function of metal oxidation state. 3. Crystal and molecular structures of tris(2,2'-bipyridine)nickel(III) triperchlorate-2-acetonitrile-0.5-dichloromethane, *Inorg. Chem.* 23 (1984) 3473–3479, <https://doi.org/10.1021/ic00190a009>.
- Z. Mtshali, J. Conradie, Tris(polypyridine)nickel(II) complexes: Synthesis, DFT and electrochemistry, *Inorganica Chim. Acta.* 549 (2023), 121422, <https://doi.org/10.1016/j.ica.2023.121422>.



- [37] J. Conradie, Redox chemistry of bis(terpyridine)manganese(II) complexes – A molecular view, *J. Electroanal. Chem.* 913 (2022), 116272, <https://doi.org/10.1016/j.jelechem.2022.116272>.
- [38] K. Wieghardt, W. Walz, B. Nuber, J. Weiss, A. Ozarowski, H. Strateimer, D. Reinen, Crystal Structure of Bis[bis(1, 4, 7-triazacyclononane)nickel(III)] Dithionate Heptahydrate and Its Single-Crystal EPR Spectrum, *Inorg. Chem.* 25 (1986) 1650–1654, <https://doi.org/10.1021/ic00230a025>.
- [39] I. Diaz-Acosta, J. Baker, J.F. Hinton, P. Pulay, Calculated and experimental geometries and infrared spectra of metal tris-acetylacetonates: vibrational spectroscopy as a probe of molecular structure for ionic complexes. Part II, *Spectrochim. Acta Part A Mol. Biomol. Spectrosc.* 59 (2003) 363–377, [https://doi.org/10.1016/S1386-1425\(02\)00166-X](https://doi.org/10.1016/S1386-1425(02)00166-X).
- [40] J. McMurtrie, I. Dance, Alternative metal grid structures formed by [M(terpy)<sub>2</sub>]<sup>2+</sup> and [M(terpyOH)<sub>2</sub>]<sup>2+</sup> complexes with small and large tetrahedral dianions, and by [Ru(terpy)<sub>2</sub>]<sup>0</sup>, *CrystEngComm.* 12 (2010) 2700, <https://doi.org/10.1039/b926074a>.
- [41] Y. Zhang, M. Zang, H. Yin, P. Liu, Y. Xian, W. Li, Dimensionally and structurally controllable perovskite single crystals: nickel(II)–terpyridine complex (Ni–Tpy 2)-based perovskites, *CrystEngComm.* 22 (2020) 1904–1908, <https://doi.org/10.1039/C9CE02004G>.
- [42] X.-P. Zhou, W.-X. Ni, S.-Z. Zhan, J. Ni, D. Li, Y.-G. Yin, From Encapsulation to Polypseudorotaxane: Unusual Anion Networks Driven by Predesigned Metal Bis(terpyridine) Complex Cations, *Inorg. Chem.* 46 (2007) 2345–2347, <https://doi.org/10.1021/ic061927o>.
- [43] J. Conradie, C.R. Ohoro, J.F. Amaku, K.O. Oyedotun, N.W. Maxakato, K. G. Akpomie, E.S. Okeke, C. Olisah, A. Malloum, K.A. Adegoke, J.O. Ighalo, Review of the structure of tris(β-diketonato)manganese complexes, *J. Mol. Struct.* 1293 (2023), 136251, <https://doi.org/10.1016/j.molstruc.2023.136251>.
- [44] D. Nyfeler, C. Hoffmann, T. Armbruster, M. Kunz, E. Libowitzky, Orthorhombic Jahn-Teller distortion and Si-OH in mozartite, CaMn<sub>3</sub>O[SiO<sub>3</sub>OH]; a single-crystal X-ray, FTIR, and structure modeling study, *Am. Mineral.* 82 (1997) 841–848, <https://doi.org/10.2138/am-1997-9-1001>.
- [45] I. Bersuker, *The Jahn-Teller Effect*, Cambridge University Press, 2006. 10.1017/CBO9780511524769.
- [46] S. Romain, C. Duboc, F. Neese, E. Rivière, L.R. Hanton, A.G. Blackman, C. Philouze, J.C. Leprêtre, A. Deronzier, M.N. Collomb, An unusual stable mononuclear Mn(III) bis-terpyridine complex exhibiting Jahn-Teller compression: Electrochemical synthesis, physical characterisation and theoretical study, *Chem. - A Eur. J.* 15 (2009) 980–988, <https://doi.org/10.1002/chem.200801442>.